JOURNAL OF ENDOUROLOGY
Volume 35, Supplement 3, December 2021

Pp. S-29–S-36
DOI: 10.1089/end.2021.0742

Mechanisms of Pulse Modulated Holmium:YAG Lithotripsy

Jason B. King, MS,[1,i] Nitesh Katta, PhD,[2] Joel M.H. Teichman, MD,[3,4]
James W. Tunnell, PhD,[1] and Thomas E. Milner, PhD[2]

Abstract

Introduction: This study aimed at answering three research questions: (1) Under the experimental conditions studied, what is the dominant mechanism of Holmium:YAG lithotripsy with or without pulse modulation? (2) Under what circumstances can laser pulse modulation increase crater volume of stone ablation per joule of emitted radiant energy? (3) Are BegoStone phantoms a suitable model for laser lithotripsy studies?
Materials and Methods: The research questions were addressed by ablation experiments with BegoStone phantoms and native stones. Experiments were performed under three stone conditions: dry stones in air, hydrated stones in air, and hydrated stones in water. Single pulses with and without pulse modulation were applied. For each pulse mode, temporal profile, transmission through 1 mm water, and cavitation bubble collapse pressures were measured and compared. For each stone condition and pulse mode, stones were ablated with a fiber separation distance of 1 mm and crater volumes were measured using optical coherence tomography.
Results: Pulses with and without pulse modulation had high (>80%) transmission through 1 mm of water. Pulses without pulse modulation generated much higher peak pressures than those with pulse modulation (62.3 *vs* 11.4 bar). Pulse modulation resulted in similar or larger craters than without pulse modulation. Trends in BegoStone crater volumes differed from trends in native stones.
Conclusions: This results of this study suggest that the dominant mechanism is photothermal with possible photoacoustic contributions for some stone compositions. Pulse modulation can increase ablation volume per joule of emitted radiant energy, but the effect may be composition specific. BegoStones showed unique infrared ablation characteristics compared with native stones and are not a suitable model for laser lithotripsy studies.

Keywords: laser lithotripsy, pulse modulation, Holmium:YAG, ablation mechanism

Introduction

Ureteroscopy is the dominant surgical management of upper tract calculi, due in part to the success of Ho:YAG lithotripsy.[1,2] The Ho:YAG laser breaks up all stone compositions and produces smaller fragments *vs* photoacoustic (pulsed dye lasers) or mechanical (LithoClast) lithotripsy devices.[3,4] Variable laser settings allows for dusting *vs* fragmentation.[5] Advances in laser technology include pulse modulation, which can increase fragmentation at a distance between the fiber tip and the stone, and reduce retropulsion.[6,7] Laser pulse modulation may also increase stone ablation even in contact mode.[8]

Ho:YAG lithotripsy experiments suggest a dominant photothermal mechanism.[9] The number of photons directed into the stone correlates with ablation crater volumes, ablation is enhanced in contact mode *vs* noncontact, and significant cavitation collapse pressures are absent.[5,10–14] Recent studies challenge the view of a dominant photothermal mechanism.[15–17] Fragmentation can be induced by water jet impingement or by cavitation bubble-induced acoustical (photoacoustic) effects. The amplitude of Ho:YAG cavitation-induced shockwaves depends on pulse duration. Pulse durations <1 μseconds yield high-amplitude expansion and collapse wave pressures. Pulse durations between 1 and $\sim$100 μseconds yield high-amplitude collapse wave pressures. Finally, longer pulse durations yield asymmetric bubbles and weak collapse pressures.[18] A range of Ho:YAG pulse durations are offered in current clinical lasers that range from 70 μs up to 400 μs or longer.

Many studies have used (artificial) stone phantoms as a surrogate for native human stones. BegoStone phantoms have similar acoustical properties as calcium oxalate monohydrate (COM) stones.[19] BegoStone phantoms are easily constructed

[1]Department of Biomedical Engineering, The University of Texas at Austin, Austin, Texas, USA.
[2]Beckman Laser Institute and Medical Clinic, University of California Irvine, Irvine, California, USA.
[3]St. Paul's Hospital, Vancouver, Canada.
[4]Department of Urologic Sciences, The University of British Columbia, Vancouver, Canada.
[i]ORCID ID (https://orcid.org/0000-0002-3866-7420).

and reproducible. Native human stones are heterogeneous in composition and geometry compared with stone phantoms. Recent work questions the suitability of BegoStone for laser lithotripsy studies due to differences in optical absorption spectra and fragmentation properties compared with native stones.[20]

In this study, we were guided by three research questions: (1) Under the experimental conditions studied, what is the dominant mechanism of Ho:YAG lithotripsy with or without pulse modulation? (2) Under what circumstances can laser pulse modulation increase stone ablation crater volume per joule of emitted radiant energy? (3) Are BegoStone phantoms a suitable model for laser lithotripsy studies?

Materials and Methods

Stone types and preparation

Four types of stones were used: BegoStone phantoms (Bego USA, Lincon, RI), COM, magnesium ammonium phosphate hexahydrate (MAPH), and uric acid anhydrous (UAA) (Louis Herring, Orlando, FL). BegoStones were prepared in 5:1 powder to water ratio by weight[21] in flat squares $\sim 25 \times 25 \times 2$ mm. BegoStones were made in a single batch to avoid batch-to-batch variation observed in preliminary experiments. De-identified human stones were purchased from an external source. Native human stone types were cut by diamond saw to produce planar ablation surfaces. For all hydrated stone experiments, the stones were immersed in distilled water for at least 72 hours at room temperature. For dry stone experiments, stones were allowed to dry in open air for >1 week at room temperature.

Experimental conditions

Three experimental conditions were compared for all stone compositions (Fig. 1A): (1) dry stones in air (dry-air); (2) hydrated stones in air (wet-air); (3) and hydrated stones in water (wet-water).

Pulse modes

A Ho:YAG laser was used as a pulsed radiant source for stone ablation (MOSES Pulse 120H; Lumenis, Yokneam, Israel). Three pulse mode groups were employed: (1) Moses distance (MD) 1 J single pulse; (2) non-Moses short pulse (NM) duration in a single 1 J pulse; and (3) non-Moses short pulse duration consisting of two 0.5 J pulses separated by at least 2 seconds (NM2 × 0.5 J). For native stones the NM2 × 0.5 J pulse mode was applied only for the dry air condition due to limited supply. An optical fiber (MOSES 200 D/F/L; Lumenis) was used for all experiments described in this article. All experiments were completed at a 1 mm fiber standoff distance to allow exploration of the clinically relevant contributions of radiant energy transmission and cavitation wave pressure to stone ablation.

Laser pulse temporal profile and transmission measurements

Temporal profiles emitted from the laser exiting the fiber for each of the three pulse modes was measured with an InGaAs photoreceiver (2034; New Focus, San Jose, CA) connected to a 200 MHz oscilloscope (TDS2024B; Tektronix, Beaverton, OR). Temporal profile was measured 10 times for each pulse mode. The full width at half maximum (FWHM) duration was calculated from the profiles. For MD the FWHM was measured from the earliest to latest half-maximum.

Temporal profiles of radiant energy transmitted through 1 mm water were measured by placing the fiber tip 1 mm from the bottom of a glass tank with the photoreceiver placed directly below the tank. Each measurement was repeated five times for each pulse mode. Mean profiles through air and through 1 mm water were compared. Transmission through 1 mm of water was measured using a power meter (PM10; Coherent, Santa Clara, CA) placed directly below the tank. The laser was fired at 5 Hz until the power meter reading reached a steady value. Measurements were repeated five times for each pulse mode. Power readings were divided by the repetition rate to calculate average transmitted pulse energy. Pulse energy was corrected for reflection and absorption losses through the glass tank to estimate the pulse energy transmission through 1 mm water.

Pressure transient measurement

For each pulse mode a pressure sensor (112A21; PCB Piezotronics, Depew, NY) connected to the 200 MHz oscilloscope was used to measure pressure transients. The Moses fiber was directed toward the pressure sensor with a 5 mm

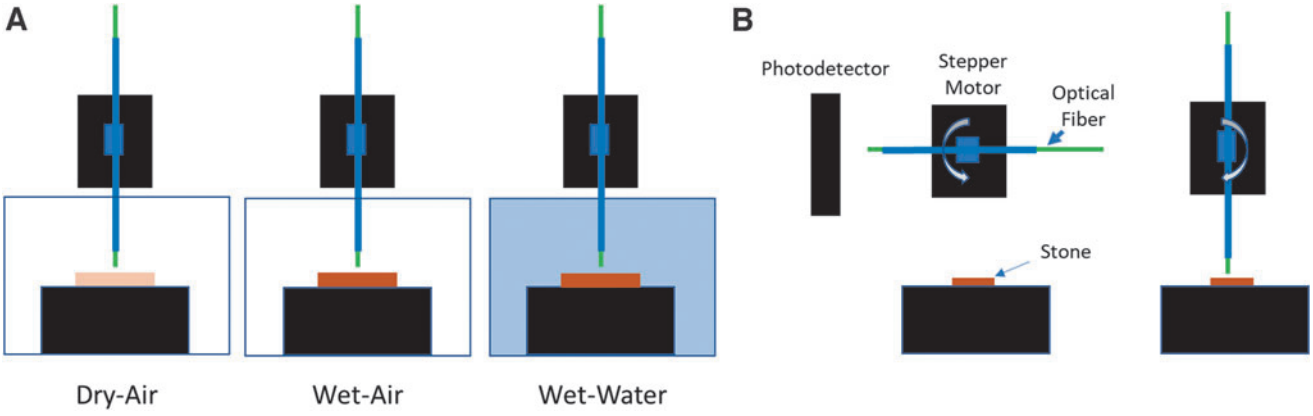

FIG. 1. Experiment setup. **(A)** Three experimental conditions were used. Dry stones surrounded by air (dry-air), hydrated stones surrounded by air (wet-air), and hydrated stones surrounded by water (wet-water). **(B)** A rotational stepper motor was used to deliver a single pulse to each stone at a fiber separation distance of 1 mm.

Table 1. Number of BegoStone Experiment Repetitions for Each Experimental Condition and Pulse Mode

Condition	*1 J NM*	*1 J MD*	*2×0.5 J NM*
Dry-air	10	10	10
Wet-air	10	10	10
Wet-water	10	10	10

MD = Moses distance; NM = non-Moses short pulse.

separation distance to prevent laser damage to the sensor surface. The pressure at 1 mm separation distance was then calculated. Pressure transients were measured 10 times for each pulse mode.

Stone ablation experiments

Single pulses were delivered to each stone ablation site. A custom-built motorized rotational actuator positioned the optical fiber tip above the stone. The motorized rotational actuator allowed delivery of a single light pulse on the stone from a train of pulses to ensure the laser output stability before ablation (Fig. 1B). The optical fiber was held in a carbon fiber tube fastened to the shaft of a stepper motor (17md302s-00; Anaheim Automation, Anaheim, CA). At the start of the experiment, the optical fiber was directed orthogonal to the stone surface-normal so that emitted Ho:YAG radiation entered an InGaAs photodetector (2034; New Focus). The laser was set to a 5 Hz repetition rate. The photodetector registered the first pulse in the pulse train and after a fixed delay (1 second), the stepper motor rotated the fiber tip toward the stone surface. Fiber rotation stopped when the fiber tip was directly above the stone surface (1 mm) and before laser emission of the subsequent pulse.

After delivery of a single pulse to the stone surface and before the following pulse, the rotational stepper motor moved the fiber tip back to the original position with the fiber directed at the photodetector. Reliable and repeatable delivery of a single laser pulse to the stone surface was verified in both air and water by observation of videos recorded with a high-speed camera (Fastcam Mini UX100; Photron, Tokyo, Japan). All pulses were delivered to both phantom and native human stones in air and water with a separation of 1 mm between the fiber tip and the stone surface. The number of repetitions for each stone type, experimental condition, and pulse mode are shown (Tables 1–4). Ten repetitions were completed for each combination of stone composition, experimental condition, and pulse mode with the exception of COM and UAA hydrated stones in water, which were limited to five repetitions due to limited stone supply. The distal end of the optical fiber was freshly cleaved after each repetition to ensure a clean fiber tip for delivery of every ablation pulse. An equal number of MD and NM experiments were completed on each stone for control.

Table 2. Number of Calcium Oxalate Monohydrate Experiment Repetitions for Each Experimental Condition and Pulse Mode

Condition	*1 J NM*	*1 J MD*	*2×0.5 J NM*
Dry-air	10	10	10
Wet-air	5	5	0
Wet-water	10	10	0

Table 3. Number of Magnesium Ammonium Phosphate Hexahydrate Experiment Repetitions for Each Experimental Condition and Pulse Mode

Condition	*1 J NM*	*1 J MD*	*2×0.5 J NM*
Dry-air	10	10	10
Wet-air	10	10	0
Wet-water	10	10	0

Crater imaging and analysis

Ablation crater volumes were measured using a custom-built optical coherence tomography (OCT) system.[22] The OCT system used a single-mode optical fiber with a swept source laser (1310 nm; Axsun, Billerica, MA). The OCT system used a Mach-Zehnder fiber interferometer configuration collecting field of views 6.5 mm (X) × 6.5 mm (Y) × 3 mm (depth). Three-dimensional tomograms were recorded after single-pulse laser irradiation of each stone type. A custom MATLAB program was used to detect the stone surface from recorded OCT data, calculate crater volume, and display a 3D reconstruction for each crater surface resulting from single-pulse laser ablation.

Ablation crater volumes across experimental conditions and pulse modes were compared by analysis of variance. When statistically significant differences ($p < 0.05$) were observed, Tukey's honest significant difference test was completed *post hoc* to determine which experimental conditions and pulse modes were statistically significant between cohorts.

Results

Laser pulse temporal profile and transmission measurements

Laser temporal profiles transmitted through air and through 1 mm water are shown (Fig. 2). The FWHM in air was 71 ± 7 μseconds for the 1 J NM, 69 ± 9 μseconds for a single 0.5 J NM short pulse, and 381 ± 13 μseconds for the 1 J MD pulse. Most of the pulse energy is emitted toward the beginning of the pulse with a tail of energy emitted at the end of the pulse. Therefore, the reported optical FWHM may be shorter than other methods of quantifying pulse duration such as full pulse duration or electrical pulse duration, which may be reported elsewhere. The profiles through 1 mm water show that the first portion of the pulse is used to form a vapor bubble and is not transmitted. Transmitted pulse energy through 1 mm water was 0.81 ± 0.04 J for NM, 0.60 ± 0.04 J for 2×0.5 J NM, and 0.84 ± 0.03 J for MD.

Table 4. Number of Uric Acid Anhydrous Experiment Repetitions for Each Experimental Condition and Pulse Mode

Condition	*1 J NM*	*1 J MD*	*2×0.5 J NM*
Dry-air	10	10	10
Wet-air	5	5	0
Wet-water	10	10	0

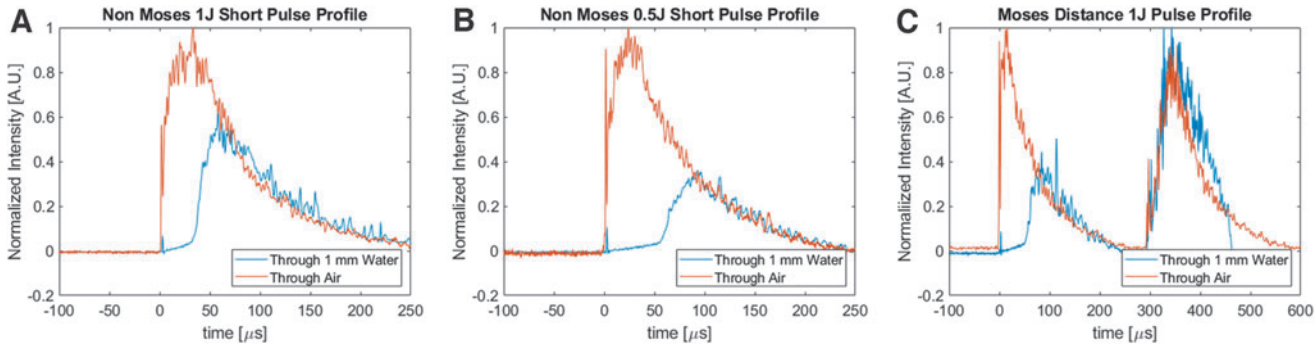

FIG. 2. Pulse duration traces transmitted in air and through 1 mm water for the three pulse modes used in this study 1 J NM **(A)**, 0.5 J NM **(B)**, and 1 J MD **(C)**. Profiles through air were normalized to a peak value of 1 and profiles through water were normalized to overlap with air profiles. Percent transmission through water is displayed on each plot. MD = Moses distance; NM = non-Moses short pulse.

Pressure transient measurement

Pressures 1 mm from the fiber tip were 62.3 ± 12.4 bars for NM, 43.1 ± 8.6 bars for 2 × 0.5 J NM, and 11.4 ± 6.7 bars for MD. Representative pressure transients are shown (Fig. 3)

Crater imaging and analysis

Representative OCT crater cross-sectional scans (B-scans) and reconstructed 3D volumes for each of the four stone types are shown (Fig. 4).

Mean ablation volumes differed across stone compositions (Fig. 5, Tables 5, and 6).

For BegoStones, MD pulses resulted in larger crater volumes compared with both NM and 2 × 0.5 J NM. NM crater volumes were significantly larger than 2 × 0.5 J NM for the wet-water case only. The rank order from largest to smallest crater volumes was dry-air>wet-air>wet-water for all three pulse mode groups.

For COM, the only statistical difference across cohorts was MD wet-air had 53% larger ablation craters than 2 × 0.5 J NM dry air.

For MAPH, MD pulses resulted in significantly larger crater volumes than NM for only the wet-water condition. No significant differences in crater volumes were observed between pulse modes for dry-air or wet-air conditions. Wet-air crater volumes were significantly larger than dry-air for both MD and NM pulse modes. Wet-air crater volumes were significantly larger than wet-water for NM only. Wet-water crater volumes were significantly larger than dry-air for MD only.

For UAA, no significant differences were observed between pulse mode groups. Wet-air craters were significantly larger than dry-air for both MD and NM pulse modes. No significant differences were observed between wet-air crater volumes and wet-water. Wet-water crater volumes were larger than dry-air for MD only.

Discussion

Research question (1): Under the experimental conditions studied, what is the dominant mechanism of Ho:YAG lithotripsy with or without pulse modulation?

Water is an excellent chromophore for Ho:YAG radiation so that photons can readily convert liquid water into a gaseous state.[23] If unconstrained (by a stone or other material boundary) a vapor bubble can form, expand maximally, and then collapse. While bubble dynamics were not measured directly in this study, an understanding of bubble dynamics reported in other literature aids in understanding the results of this study. A combination of short pulse duration (typically <1 μseconds) and a relatively long bubble lifetime (typically hundreds of μseconds) leads to high-amplitude expanding and collapsing pressure shockwaves.[18] As the optical pulse duration lengthens up to 100 μseconds (and the bubble lifetime remains on the order of hundreds of μseconds) the

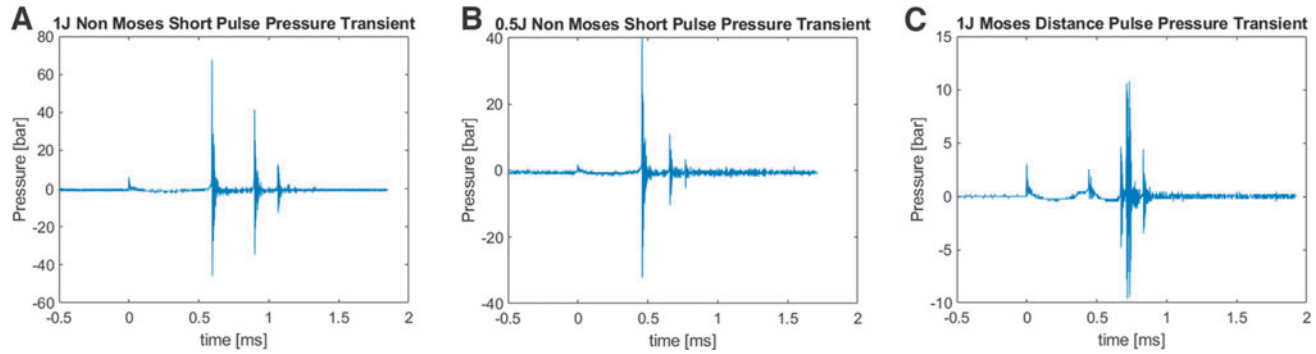

FIG. 3. Representative pressure transients for 1 J NM **(A)**, 0.5 J NM **(B)**, and 1 J MD **(C)** pulse modes. Pressure measurements were recorded 5 mm from fiber tip and corrected to pressure 1mm from fiber tip. Peak pressures are displayed as mean ± SD.

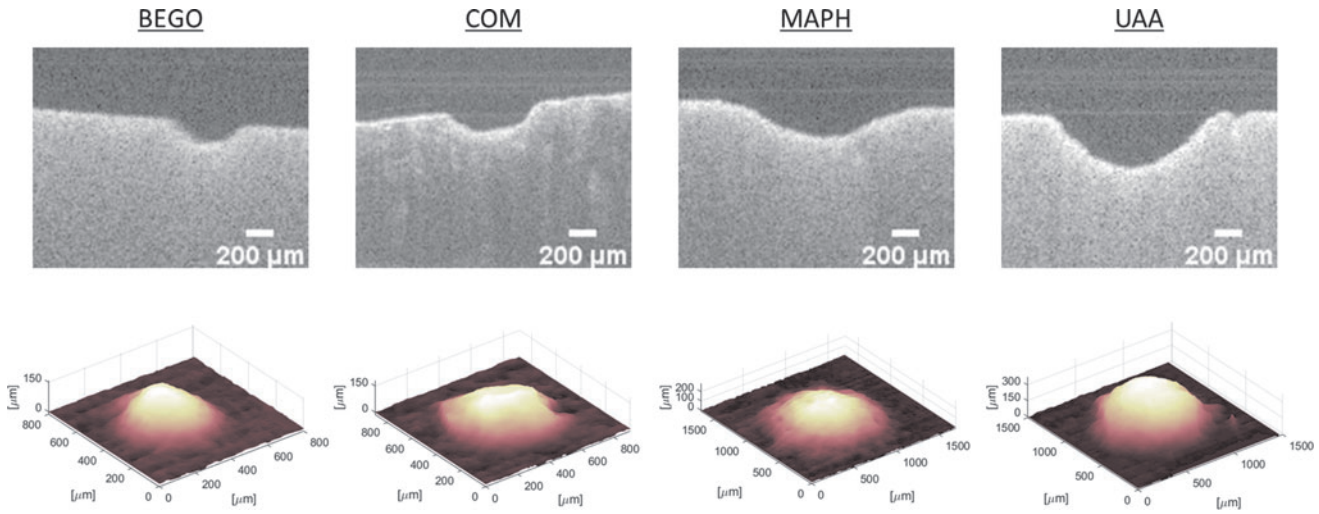

FIG. 4. Representative OCT images and 3D crater surface plots. Cases shown are for the wet-air condition with a single 1 J NM pulse. OCT, optical coherence tomography.

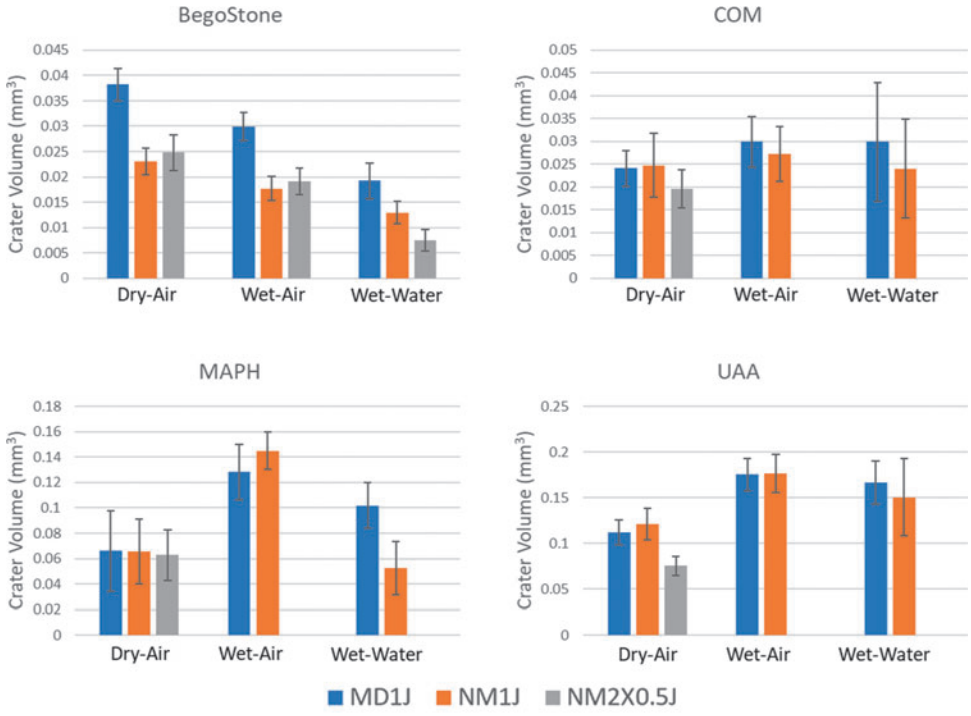

Ablation Volumes (mm³)

	MD1J	NM1J	NM2X0.5J
BegoStone Dry-Air	0.038±0.003	0.023±0.003	0.025±0.004
BegoStone Wet-Air	0.030±0.003	0.018±0.002	0.019±0.003
BegoStone Wet-Water	0.019±0.004	0.013±0.002	0.0075±0.002
COM Dry-Air	0.024±0.004	0.0250±0.007	0.020±0.004
COM Wet-Air	0.030±0.006	0.027±0.006	
COM Wet-Water	0.030±0.013	0.024±0.011	
MAPH Dry-Air	0.066±0.032	0.066±0.026	0.063±0.020
MAPH Wet-Air	0.128±0.022	0.145±0.015	
MAPH Wet-Water	0.102±0.018	0.053±0.021	
UAA Dry-Air	0.112±0.013	0.121±0.017	0.075±0.010
UAA Wet-Air	0.176±0.018	0.176±0.021	
UAA Wet-Water	0.167±0.024	0.151±0.042	

FIG. 5. Ablation volumes for each stone type, experimental condition, and pulse mode. Data are displayed as mean ± SD.

Table 5. *P*-Values for Pulse Mode Comparisons for Each Experimental Condition from Tukey's Honest Significant Difference Test

Type of stone	*Experimental condition*	*Pulse mode comparison*	p
BegoStone	Dry-air	NM *vs* MD	<0.001
		NM *vs* 2×0.5 J NM	0.9
		MD *vs* 2×0.5 J NM	<0.001
	Wet-air	NM *vs* MD	<0.001
		NM *vs* 2×0.5 J NM	<0.001
		MD *vs* 2×0.5 J NM	<0.001
	Wet-water	NM *vs* MD	<0.001
		NM *vs* 2×0.5 J NM	0.007
		MD *vs* 2××0.5 J NM	<0.001
COM	Dry-air	NM *vs* MD	>0.9
		NM *vs* 2×0.5 J NM	0.6
		MD *vs* 2×0.5 J NM	0.8
	Wet-air	NM *vs*. MD	>0.9
	Wet-water	NM *vs*. MD	0.8
MAPH	Dry-air	NM *vs* MD	>0.9
		NM *vs* 2×0.5 J NM	>0.9
		MD *vs* 2×0.5 J NM	>0.9
	Wet-air	NM *vs*. MD	0.6
	Wet-water	NM *vs* MD	<0.001
UAA	Dry-air	NM *vs* MD	>0.9
		NM *vs* 2×0.5 J NM	0.009
		MD *vs* 2×0.5 J NM	0.07
	Wet-air	NM *vs* MD	>0.9
	Wet-water	NM *vs* MD	0.9

COM = calcium oxalate monohydrate; MAPH = magnesium ammonium phosphate hexahydrate; UAA = uric acid anhydrous.

Table 6. *P*-Values for Experimental Condition Comparisons for Pulse Mode from Tukey's Honest Significant Difference Test

Type of stone	*Pulse mode*	*Experimental condition comparison*	p
BegoStone	Non-Moses NM	Dry-air *vs* wet-air	0.002
		Wet-air *vs* wet-water	0.009
		Dry-air *vs* wet-water	<0.001
	Moses distance	Dry-air *vs* wet-air	<0.001
		Wet-air *vs* wet-water	<0.001
		Dry-air *vs* wet-water	<0.001
	2×0.5 J NM	Dry-air *vs*. wet-air	<0.001
		Wet-air *vs* wet-water	<0.001
		Dry-air *vs* wet-water	<0.001
COM	Non-Moses NM	Dry-air *vs* wet-air	>0.9
		Wet-air *vs* wet-water	>0.9
		Dry-air *vs*. wet-water	>0.9
	Moses distance	Dry-air *vs* wet-air	0.5
		Wet-air *vs* wet-water	>0.9
		Dry-air *vs* wet-water	0.7
MAPH	Non-Moses NM	Dry-air *vs* wet-air	<0.001
		Wet-air *vs* wet-water	<0.001
		Dry-air *vs* wet-water	0.8
	Moses distance	Dry-air *vs* wet-air	<0.001
		Wet-air *vs* wet-water	0.13
		Dry-air *vs* wet-water	0.012
UAA	Non-Moses NM	Dry-air *vs*. wet-air	<0.001
		Wet-air *vs* wet-water	0.3
		Dry-air *vs* wet-water	0.17
	Moses distance	Dry-air *vs* wet-air	<0.001
		Wet-air *vs* wet-water	>0.9
		Dry-air *vs*. wet-water	<0.001

bubble expansion remains spherical and may yield significant amplitude collapse pressure (shockwave) but not high-amplitude expansion pressure (shockwave).

With further prolongation of the pulse duration, photons continue to expand the bubble, which becomes progressively asymmetric and collapses at various loci at different times (yielding minimal amplitude collapse pressure). In the presence of a stone (or nearby material boundary) the bubble expansion is perturbed and asymmetric with less chance for cavitation-induced shockwaves. Thus, in the laser lithotripsy settings, with an optical fiber directing Ho:YAG photons at a kidney stone in an aqueous environment, either cavitation-induced photoacoustic activity *vs* direct photon absorption by the stone can occur depending on pulse duration, bubble geometry, number of pulses delivered, and proximity of the fiber to the stone. In direct photon absorption, on the other hand, photons may be absorbed primarily by either minerals in the stone or water molecules in the stone interstices.

Our data show that a high percentage of the pulse energy is transmitted through 1 mm water for both the NM (81%) and MD (84%) pulse modes, while the pressure generated was much higher for NM (62.3 bar) than for MD (11.4 bar). Therefore, if the single-pulse ablation were dominated by a photoacoustic mechanism, we might expect NM craters to be larger than MD for the wet-water condition. MD resulted in similar or larger craters suggesting ablation is dominated by a photothermal mechanism.

Hydrated native stones had similar or greater ablation volumes than dry stones suggesting that absorption by water in the stone enhances ablation.

Our data suggest that with BegoStones, the predominant ablation mechanism is photothermal. Large volume ablation craters are observed regardless of dry-air *vs* wet-air or wet-water experimental conditions. In the dry-air and wet-air conditions, negligible acoustic energy is generated in the air above the stone and most radiant energy transfer is within the stone. COM stones show no difference between each of these three stone experimental conditions (dry-air, wet-air, or wet-water), implying no additional ablation due to water or cavitation. These results are consistent with a photothermal mechanism. The MAPH stones showed more ablation in wet-air condition over dry-air or wet-water, implying possible explosive vaporization in the stone. We infer that MAPH stones in water have a much higher water content than COM such that water becomes the dominant chromophore. Likewise, UAA showed equal ablation advantage of wet-air and wet-water over dry-air.

The evidence that single-pulse Ho:YAG lithotripsy studied here works predominantly by a photothermal mechanism (direct photon absorption either by the stone and/or water within the stone) is supported by previous experiments.[8,9,11,14,18,24] Most Ho:YAG lasers in clinical lithotripsy have optical pulse durations generally ranging from 70 to 400 μseconds. There is an absence of any demonstrable expansion pressure transient (i.e., no expansion shockwave), relatively low-amplitude collapse pressures (generally 20-60 bars in still water), asymmetric bubble expansion, and multiple collapse loci (in contrast to Q-switched, pulsed dye lasers, and electrohydraulic lithotripsy, which collapse to a single focus with higher collapse pressures).

Furthermore, measured ablation crater volumes correlate with fluence.[12] Maximum ablation crater volume occurs when the fiber is in contact with the stone. Larger ablation crater volumes are observed when the stone is irradiated in air *vs* water (whether the stone is dry or hydrated). In the air cases, stone fragmentation is associated with thermal breakdown products that can only occur with photons heating the stone to a critically high temperature.[8,9] Shalini and colleagues performed a series of experiments with COM and synthetic struvite stones comparing regular water and deuterium (heavy water) effects. Changing the absorption of the stones at 2.12 μm changes the extent of fragmentation, whereas changing the absorption of the bulk medium has a negligible effect on fragmentation. These results further support a photothermal lithotripsy mechanism.[24]

Although the studies described did not directly investigate the photoacoustic mechanism to stone ablation, our results and analysis may provide a useful perspective to better evaluate the relative contribution of photothermal/photoacoustic effects in laser lithotripsy. The evidence that Ho:YAG lithotripsy works predominantly by a photoacoustic mechanism has recently been advanced.[13–15] In these experiments, Ho:YAG ablation is greatest when the stone is hydrated and there is water coupling the fiber to the stone. Ho:YAG ablation occurs when the fiber is oriented parallel to the stone surface (so that minimal or no photons can reach the stone) by a known cavitation bubble phenomena whereby water jets from the collapse of the bubble if at a ''sweet spot'' distance away from a nearby boundary. The stone is not too close to and not too far from the fiber and bubble.[25] When the pulse duration is short (on the order of 75 μseconds in these experiments), the cavitation bubble remains relatively spherical, which leads to high collapse pressures capable of inducing shockwaves.[17,18]

While many experiments supporting a photothermal mechanism studied the effects of a single-pulse ablation, the experiments supporting photoacoustic mechanism studied the effects of multiple pulses impacting the same location.[7,14,15] Stone fracture may be susceptible to multiple small-amplitude pressure waves if a sufficient number of pulses are directed to the same stone location. Other experiments show the opposite phenomena: a law of diminishing returns is observed with multiple pulses at the same location reaching a maximum ablation effect and no further ablation achieved with additional pulses at the same location.[26]

Research question (2): Under what circumstances can laser pulse modulation increase crater volume of stone ablation per joule of emitted radiant energy?

An interesting feature of our data was the ability of pulse modulation to produce 40% greater ablation crater volumes than a single pulse of the same energy (in a BegoStone). This ablation advantage was not observed when we irradiated the identical stone location with two individual pulses separated by seconds with a combined energy equal to that of the modulated pulse. We infer that the observed increased ablation crater volume from pulse modulation is dependent on the delay between the two pulses. When the delay is synchronized so the initial bubble is followed by a second bubble at a specified delay time, increased ablation crater volume was observed. A similar magnitude ablation advantage with pulse modulation was not observed with COM, MAPH, or UAA stones for dry-air conditions. The ablation advantage of using pulse modulation in contact mode may be composition specific.[6]

Pulse modulation also creates unusual, complex, and asymmetric bubbles. The initial bubble expands and begins its collapse while the second pulse is emitted leading to an hourglass-shaped bubble with more forward expansion than seen with a single pulse and its characteristic pear-shaped bubble.[8,27] With pulse modulation, evidence points to a long pulse duration, low pressure transients, and a relatively higher ratio of pulse duration to bubble lifetime (compared with single short pulse durations).

For all stone compositions, pulse modulation showed advantages of ablation crater volumes for equal pulse energies (1 J pulse modulation over 1 J NM at 1 mm distance). Thus, the concept that pulse modulation can give a longer ''strike-reach'' of photons to cross a water gap between the fiber tip and the stone surface is supported by our data.[8,28]

Ablation trends are composition specific and dependent on the fluence and fluence decreases with increased fiber separation distance. Therefore, ablation trends between stone compositions and pulse modes may vary with fiber separation distance. This study was limited to one separation distance due to limited availability of native stones.

Research question (3): Are BegoStone phantoms a suitable model for laser lithotripsy studies?

Our data show BegoStones respond differently to infrared radiation than any native human stone tested. BegoStones yield different ablation crater volumes at each condition tested, and different patterns of ablation with different conditions. Photon absorption and ablation efficiency are composition specific.[28] Better elucidation of differences between the response of BegoStones and native stones in laser lithotripsy may be gained by characterizing their optical properties.

Conclusions

The mechanism of Ho:YAG lithotripsy varies with experimental conditions. With some compositions and conditions, photothermal is dominant. With other compositions, it appears to be photothermal with some photoacoustic contribution as water contributes to increased ablation. The pulse duration also plays a key role in fragmentation mechanism. Pulse modulation can increase ablation volumes per joule of emitted radiant energy in BegoStones, but may be composition specific. BegoStones have unique, different laser ablation characteristics compared with human stones and are not an ideal model for laser lithotripsy studies.

Author Disclosure Statement

Dr. Teichman is a consultant for Boston Scientific, Cook Urologic, and Lumenis.

Funding Information

This project was partially funded by a grant from Lumenis. J. King was partially funded by a training grant from the National Institutes of Health, Grant #T32EB007507.

References

1. Oberlin DT, Flum AS, Bachrach L, et al. Contemporary surgical trends in the management of upper tract calculi. J Urol 2015;193:880–884.
2. Aldoukhi AH, Roberts WW, Hall TL, et al. Holmium laser lithotripsy in the new stone age: Dust or bust? Front Surg 2017;4:57.

3. Razvi HA, Denstedt JD, Chun SS, et al. Intracorporeal lithotripsy with the holmium: YAG laser. J Urol 1996;156: 912–914.
4. Teichman JMH, Vassar GJ, Bishoff JT, et al. Holmium: YAG lithotripsy yields smaller fragments than lithoclast, pulsed dye laser or electrohydraulic lithotripsy. J Urol 1998;159:17–23.
5. Sea J, Jonat LM, Chew BH, et al. Optimal power settings for Holmium:YAG lithotripsy. J Urol 2012;187:914–919.
6. Elhilali MM, Badaan S, Ibrahim A, et al. Use of the Moses technology to improve holmium laser lithotripsy outcomes: A preclinical study. J Endourol 2017;31:598–604.
7. Black KM, Aldoukhi AH, Teichman JMH, et al. Pulse modulation with Moses technology improves popcorn laser lithotripsy. World J Urol 2021;39:1699–1705.
8. Aldoukhi AH, Roberts WW, Hall TL, et al. Watch your distance: The role of laser fiber working distance on fragmentation when altering pulse width or modulation. J Endourol 2019;33:120–126.
9. Chan KF, Vassar GJ, Pfefer TJ, et al. Holmium: YAG laser lithotripsy: A dominant photothermal ablative mechanism with chemical decomposition of urinary calculi. Lasers Surg Med 1999;25:22–37.
10. Vassar GJ, Teichman JMH, Glickman RD. Holmium: YAG lithotripsy efficiency varies with energy density. J Urol 1998;160:471–476.
11. Beghuin D, Delacretaz GP, Schmidlin FR, et al. Fragmentation process during Ho: YAG laser lithotripsy revealed by time-resolved imaging. In: Laser-Tissue Interaction, Tissue Optics, and Laser Welding III. Vol. 3195. Proc. SPIE 1998, pp. 220–224.
12. Lee H, Ryan RT, Teichman JMH, et al. Effect of lithotripsy on Holmium:YAG optical beam profile. J Endourol 2003; 17:63–67.
13. Lee HO, Ryan RT, Teichman JMH, et al. Stone retropulsion during holmium: YAG lithotripsy. J Urol 2003;169: 881–885.
14. Zhong P, Tong H-L, Cocks FH, et al. Transient cavitation and acoustic emission produced by different laser lithotripters. J Endourol 1998;12:371–378.
15. Taratkin M, Laukhtina E, Singla N, et al. How lasers ablate stones: In vitro study of laser lithotripsy (Ho: YAG and Tm-Fiber Lasers) in different environments. J Endourol 2021;35:931–936.
16. Ho DS, Scialabba D, Terry RS, et al. The role of cavitation in energy delivery and stone damage during laser lithotripsy. J Endourol 2021;35:860–870.
17. Ho D, Chen J, Xiang G, et al. PD54-09 significant contribution of cavitation to dusting stone damage in laser lithotripsy. J Urol 2021;206:e926.
18. Jansen ED, Asshauer T, Frenz M, et al. Effect of pulse duration on bubble formation and laser-induced pressure waves during holmium laser ablation. Lasers Surg Med 1996;18:278–293.
19. Esch E, Simmons WN, Sankin G, et al. A simple method for fabricating artificial kidney stones of different physical properties. Urol Res 2010;38:315–319.
20. Frank DS, Aldoukhi AH, Roberts WW, et al. Polymer–mineral composites mimic human kidney stones in laser lithotripsy experiments. ACS Biomater Sci Eng 2019;5:4970–4975.
21. Liu Y, Zhong P. BegoStone—a new stone phantom for shock wave lithotripsy research (L). J Acoust Soc Am 2002;112:1265–1268.
22. Katta N, McElroy AB, Estrada AD, et al. Optical coherence tomography image-guided smart laser knife for surgery. Lasers Surg Med 2018;50:202–212.
23. Jansen ED, van Leeuwen TG, Motamedi M, et al. Temperature dependence of the absorption coefficient of water for midinfrared laser radiation. Lasers Surg Med 1994;14: 258–268.
24. Shalini S, Frank DS, Aldoukhi AH, et al. Assessing the role of light absorption in laser lithotripsy by isotopic substitution of kidney stone materials. ACS Biomater Sci Eng 2020;6:5274–5280.
25. Lauterborn W, Bolle H. Experimental investigations of cavitation-bubble collapse in the neighbourhood of a solid boundary. J Fluid Mech 1975;72:391–399.
26. Aldoukhi AH, Black KM, Hall TL, et al. Frequency threshold for ablation during holmium laser lithotripsy: How high can you go? J Endourol 2020;34:1075–1081.
27. Terry RS, Ho DS, Scialabba DM, et al. Comparison of different pulse modulation modes for Holmium: Yttrium-Aluminum-Garnet laser lithotripsy ablation in a Benchtop model. J Endourol 2022; DOI: 10.1089/end.2021.0113.
28. Chan KF, Hammer DX, Choi B, et al. Free electron laser lithotripsy: Threshold radiant exposures. J Endourol 2000; 14:161–167.

Address correspondence to:
Jason B. King, MS
Department of Biomedical Engineering
The University of Texas at Austin
107 W Dean Keeton Street
Austin, TX 78712
USA

E-mail: jason.b.king@utexas.edu

Abbreviations Used

COM = calcium oxalate monohydrate
FWHM = full width at half maximum
Ho:YAG = Holmium:Yttrium–Aluminum–Garnet
MAPH = magnesium ammonium phosphate hexahydrate
MD = Moses distance
NM = Non-Moses short pulse
NM2×0.5J = Non-Moses two repeated 0.5J short pulses
OCT = optical coherence tomography
UAA = uric acid anhydrous